NASA TM X-2884

NASA TECHNICAL MEMORANDUM

NASA TM X-2884

ANALYSIS OF A WATER TABLE SIMULATION OF A TRANSPIRATIONALLY COOLED NOZZLE

by Albert F. Kascak

Lewis Research Center
Cleveland, Ohio 44135

NATIONAL AERONAUTICS AND SPACE ADMINISTRATION • WASHINGTON, D. C. • OCTOBER 1973

1. Report No.	2. Government Accession No.	3. Recipient's Catalog No.
NASA TM X-2884		

4. Title and Subtitle	5. Report Date
ANALYSIS OF A WATER TABLE SIMULATION OF A TRANSPIRATIONALLY COOLED NOZZLE	October 1973
	6. Performing Organization Code

7. Author(s)	8. Performing Organization Report No.
Albert F. Kascak	E-7524
	10. Work Unit No. 503-04

9. Performing Organization Name and Address	11. Contract or Grant No.
Lewis Research Center National Aeronautics and Space Administration Cleveland, Ohio 44135	

12. Sponsoring Agency Name and Address	13. Type of Report and Period Covered
National Aeronautics and Space Administration Washington, D.C. 20546	Technical Memorandum
	14. Sponsoring Agency Code

15. Supplementary Notes

16. Abstract

This study formulates two flow models - for a no-mixing and a complete-mixing boundary layer. The approach taken assumes inviscid flow and constant pressure in the transverse direction. The models are simple enough so that extending them to apply to a gas nozzle, including heat transfer and density differences, should be possible. Both models predict experimental photographic data with similar results; but inherent two-dimensional and parallax errors preclude choice of the best model. In general, the boundary layer thickens rapidly near the start of injection because of low acceleration forces; it thins near the throat because of high acceleration forces. The transpiration fluid increases the radius of curvature near the throat and decreases the divergence angle of the free flow downstream of the throat.

17. Key Words (Suggested by Author(s))	18. Distribution Statement
Water table Transpiration Nozzle Heat transfer	Unclassified - unlimited

19. Security Classif. (of this report)	20. Security Classif. (of this page)	21. No. of Pages	22. Price*
Unclassified	Unclassified	25	Domestic, $2.75 Foreign, $5.25

* For sale by the National Technical Information Service, Springfield, Virginia 22151

ANALYSIS OF A WATER TABLE SIMULATION OF A TRANSPIRATIONALLY COOLED NOZZLE

by Albert F. Kascak

Lewis Research Center

SUMMARY

This report contains an analysis of a water table simulation of a transpirationally cooled nozzle. Two flow models of the water table boundary layer are formulated and then analyzed to predict experimental results. The approach taken is to assume that the pressure is constant in the transverse direction and dictated by the main flow. It is also assumed that the flow is inviscid and that there is no mixing between the injected flow and the main flow.

The first model analyzed is one in which there is no mixing in the boundary layer, and the second model analyzed is one in which there is complete mixing in the boundary layer. The models are simple enough so that extending them to apply to a gas nozzle, including density differences and heat transfer, should be possible.

The results of this analysis are presented in the form of four relations. The first is a relation governing the flow through any water table channel; the other three are relations governing the boundary layer thickness, mass, and momentum. The equations are coupled by the fact that the free-flow channel is equal to the physical channel minus the boundary layer thickness. If the flow is not choked, the height of the main flow at the start of injection is an independent parameter and the problem is an initial-value problem. If the flow is choked, the height of the main flow at the start of injection is dependent on the area of the throat. The area of the throat is unknown since the boundary layer is unknown. The problem then becomes a two-point boundary value problem.

Both models predict the photographic data with similar results; but inherent two-dimensional and parallax errors preclude choice of the best model. The largest difference in the two models occurs in the boundary layer thickness, with less of a difference in boundary layer momentum and only a slight difference in boundary layer mass.

Transpiration flows of the order of a few percent of the main flow result in only slight perturbations of the main flow, while transpiration flows of the order of tens of percent result in major changes. In general, the boundary layer thickens rapidly near the start of injection because of low acceleration forces, while it thins near the throat because of high acceleration forces. The transpiration fluid increases the radius of curvature near the throat and decreases the divergence angle of the free flow downstream of the throat. Thus, the design of a transpirationally cooled nozzle can incorporate a smaller radius of curvature at the throat and a large divergence angle.

INTRODUCTION

Advanced propulsion devices such as the gas-core nuclear rocket have predicted specific-impulse capabilities between 2000 and 7000 seconds (ref. 1). Regenerative cooling may not be able to cool these high-specific-impulse nozzles (ref. 2). A possible way to cool these nozzles may be by transpiration (ref. 3). A coolant first cools the wall as it passes through it and then forms an insulating layer adjacent to the wall.

The interaction of the transpiration coolant and the hot propellant is a complicated phenomenon. In order to get insight into this problem, a water table simulation of a transpirationally cooled nozzle was used for flow visualization studies by H. C. Perkins and R. B. Kinney of Arizona University under NASA grant NGR-03-002-213. (There is an analogy between compressible flow through a nozzle and flow over a water table, ref. 4.)

This study formulates two analytical flow models of the water table (with transpirational flow) and then analyzes these models to predict the experimental results. The approach taken is to assume that the pressure is constant in the transverse direction and is dictated by the main flow. It is also assumed that there is no mixing between the injected flow and the main flow. The first model analyzed is one in which there is no mixing in the boundary layer, and the second model analyzed is one in which there is complete mixing in the boundary layer.

ANALYSIS

A water table which is used to simulate a transpirationally cooled nozzle is shown in figure 1. The water table is a level surface with convergent-divergent vertical side walls. The level surface and the side walls form a channel (open on the top) through which water flows. Transpirational fluid flows from a plenum outside the convergent-divergent channel walls, through the permeable channel walls, and into a boundary layer adjacent to the channel walls. All the fluid in the boundary layer is transpiration fluid and comes through the side channel walls. The surface separating the main flow from the boundary layer is assumed to be parallel to the channel wall. The height of the fluid in the boundary layer is equal to the height of the main stream. The flow area through the channel wall is limited by a liner to the height of the main stream.

The main flow analysis is given in reference 5 and is only sketched herein to show the simularities between the main flow and the boundary layer.

The flow area is

$$A = bh \tag{1}$$

(All symbols are defined in the appendix.) For steady-state, incompressible, inviscid, one-dimensional flow the continuity and momentum equations are

$$\dot{m} = \rho v A = \rho v b h = \text{constant} \tag{2}$$

$$\frac{d\dot{M}}{dz} = -\frac{\rho g}{2}\frac{d}{dz}(bh^2) + \frac{\rho g}{2}h^2\frac{db}{dz} \tag{3}$$

Where the average pressure is $1/2\ \rho gh$ and the terms on the right side of the momentum equation represent the forces acting. The first term represents the force on a control surface normal to the axis. The second term represents the axial component of the force on a control surface adjacent to the side wall of the channel. The control surface on the top of the channel is a free surface and does not contribute. The control surface on the bottom is level (or parallel with the z-axis) and does not contribute in the horizontal direction. Differentiating in equation (3) results in

$$\dot{m}\frac{dv}{dz} = -\rho g h b\frac{dh}{dz} \tag{4}$$

Substituting equation (2) into equation (4) gives

$$\rho v h b\frac{dv}{dz} = -\rho g b h\frac{dh}{dz} \tag{5}$$

Then equation (5) reduces to the standard momentum relation for a water table,

$$0 = \frac{d}{dz}(v^2 + 2gh) \tag{6}$$

Equation (6) can be integrated from a point where the velocity is zero (stagnation condition) to any arbitrary point,

$$v^2 = 2g(h_s - h) \tag{7}$$

Equation (7) can be substituted into equation (2) and the results can be written as

$$0 = \left(\frac{h}{h_s}\right)^3 - \left(\frac{h}{h_s}\right)^2 + \frac{1}{2gh_s^3}\left(\frac{\dot{m}}{\rho b}\right)^2 \tag{8}$$

This cubic equation has the following solutions:

$$\frac{h}{h_s} = \frac{1}{3} + \frac{2}{3}\cos\left(\frac{\varphi + 2\pi k}{3}\right) \tag{9a}$$

where

$$\varphi = \cos^{-1}\left[1 - \frac{27}{4gh_s^3}\left(\frac{\dot{m}}{\rho b}\right)^2\right] \tag{9b}$$

and k is equal to 0, 1, or 2. The boundary conditions far upstream are $h \to h_s$ as $b \to \infty$. The only value of k which meets these conditions in equation (9) is $k = 0$. The boundary conditions far downstream are $h \to 0^+$ as $b \to \infty$. The only value of k which meets these conditions in equation (9) is $k = 2$. At the throat $k = 0$ and $k = 2$ should give the same height. Therefore, φ must be equal to π and $\cos\varphi = -1$. Then from equation (9b)

$$h_s = \left(\frac{3}{2}\right)\sqrt[3]{\frac{1}{g}\left(\frac{\dot{m}}{\rho b_t}\right)^2} \tag{10}$$

Equations (7), (9a), and (10) form a complete description of a water table flow once the mass flow rate and channel width are specified.

The free-flow area is shown in figure 1 by the curves. The free-flow channel width is approximately equal to the width of the channel walls minus the boundary layer thickness on both sides. The curved flow width is approximated by the actual channel width. This is a common approximation for one-dimensional nozzle flow.

$$b = b_w - 2\delta \tag{11}$$

(There is no boundary layer on the bottom because there is no transpiration fluid injected on the bottom and the main flow is inviscid.) It is assumed that the pressure (or height) is constant in the transverse direction and is dictated by the main flow (eqs. (7), (9), and (10)). It is also assumed that there is no mixing between the main flow and the boundary layer and that the boundary layer is inviscid. The continuity and momentum equations for the boundary layer are

$$\frac{d\dot{m}_b}{dS} = 2\frac{d\dot{m}_w}{dS} \tag{12}$$

$$\frac{d\dot{M}_b}{dS} = -\frac{\rho g}{2}\frac{d}{dS}(2\delta h^2) + \frac{\rho g}{2} h^2 \frac{d}{dS}(2\delta) \tag{13}$$

Where S is the distance measured along the channel wall and the transpiration fluid has no momentum in the S direction, when it initially enters the channel. The distance along the wall can be related to the axial distance by the geometry of the channel wall,

$$dS = \sqrt{1 + \left(\frac{b'_w}{2}\right)^2}\, dz \tag{14}$$

The transpiration fluid can be considered a jet discharging from a higher pressure outside the wall to a lower pressure inside the channel wall,

$$\frac{d\dot{m}_w}{dS} = C\rho\sqrt{2g(h_p - h)}\, h \tag{15}$$

where C is the discharge coefficient and hdS is the flow area. When equations (14) and (15) are used, the continuity and momentum equations for the boundary layer become

$$\frac{d\dot{m}_b}{dz} = 2\rho C\sqrt{2g(h_p - h)}\sqrt{1 + \left(\frac{b'_w}{2}\right)^2}\, h \tag{16}$$

$$\frac{d\dot{M}_b}{dz} = -\rho g h(2\delta)\frac{dh}{dz} \tag{17}$$

There are two models used to calculate the relation between the boundary layer thickness mass and momentum. The first assumes no mixing in the boundary layer; the second assumes complete mixing in the boundary layer.

In the no-mixing boundary layer model; the boundary layer is composed of stream tubes extending from the point of injection on the channel wall and flowing adjacent to the wall and out the nozzle (fig. 2). Each stream tube behaves like a miniature nozzle, except that rather than the width being specified the pressure (or height) at each location is specified from the main flow calculations. Rewriting equation (8) in terms of this miniature nozzle and solving for its width gives

$$d\delta = \frac{d\dot{m}_w}{\rho\sqrt{2g\left(h_{s,w}h^2 - h^3\right)}} \tag{18}$$

The mass flow rate through this minature nozzle is equal to one-half the increment in the mass flow rate of the boundary layers at the point of injection,

$$d\dot{m}_w = \frac{1}{2} d\dot{m}_{b,i} = \rho C_i \sqrt{2g(h_{p,i} - h_i)}\, h_i dS_i \tag{19}$$

The subscript i represents the point of injection. The stagnation height of this miniature nozzle is just the height at the point of injection. (That is, the injected flow is normal to the wall, and the tangential velocity is zero. The normal component of the flow is small since the wall area is large, and therefore any recovery of the flow in the tangential direction can be neglected.) Symbolically, integrating equation (18) along the axis from the point at which injection starts z_0 to the point of interest z gives

$$\delta = \frac{1}{2} \int_{z_0}^{z} \left(\frac{d\dot{m}_b}{dz}\right)_i \frac{dz_i}{\rho h \sqrt{2g(h_i - h)}} \tag{20}$$

where the i subscripts denote the quantities changing in the integration. Likewise the momentum associated with this miniature nozzle is

$$d\dot{M}_b = \sqrt{2g(h_{s,w} - h)}\, d\dot{m}_w$$

Applying the same reasoning and integrating give

$$\dot{M}_b = \int_{z_0}^{z} \sqrt{2g(h_i - h)} \left(\frac{d\dot{m}_b}{dz}\right)_i dz_i \tag{21}$$

Equation (21) can be differentiated with respect to the axial distance and, when equation (20) is used, results in a restatement of equation (17). Therefore, equation (21) is not an independent relation. A complete description of the water table with transpirational boundary layers is given by the stagnation heights upstream and outside the channel walls, by the geometry, and by equations (7), (9), (10), (16), (17), and (20).

The second model analyzed is one in which there is complete mixing in the boundary layer. The boundary layer is characterized by velocity v_b. The mass flow rate is

$$\dot{m}_b = \rho v_b (2\delta) h \tag{22}$$

and the momentum associated with the mass flow rate is

$$\dot{M}_b = v_b \dot{m}_b \tag{23}$$

Equations (22) and (23) can be solved for the boundary layer thickness and velocity:

$$\delta = \frac{\dot{m}_b^2}{2\rho h \dot{M}_b} \tag{24}$$

$$v_b = \frac{\dot{M}_b}{\dot{m}_b} \tag{25}$$

Equations (7), (9), (10), (16), (17), and (24) form a complete set for this model.

The preceding equations can be nondimensionalized if a_* is defined to be a reference length and β is a constant equal to

$$\beta = \frac{\dot{m}}{2\rho a_* h_s \sqrt{2gh_s}} \tag{26a}$$

The parameters are then defined by

$$y = \frac{h}{h_s} \tag{26b}$$

$$\epsilon = \frac{h\delta}{\beta h_s a_*} \tag{26c}$$

$$\xi = \frac{z}{\beta a_*} \tag{26d}$$

$$\eta = \frac{b_w}{2\beta a_*} \tag{26e}$$

$$w = \frac{\dot{m}_b}{\dot{m}} \tag{26f}$$

$$u = \frac{M_b}{\sqrt{2gh_s}\,\dot{m}} \tag{26g}$$

$$d = \frac{\delta}{\beta a_*} \tag{26h}$$

Substituting equations (11) and (26) into (8) yields

$$\epsilon = y\eta - \frac{1}{\sqrt{1 - y}} \tag{27}$$

Substituting equations (26) into (16) and (17) yields

$$\frac{d_w}{d\xi} = Cy\sqrt{y_p - y}\sqrt{1 + (\eta')^2} \tag{28}$$

$$\frac{du}{d\xi} = -\frac{\epsilon}{2}\frac{dy}{d\xi} \tag{29}$$

where η the channel geometry, C the discharge coefficient, y_p the stagnation height outside the channel wall are given functions of ξ. Substituting equations (26) into equation (20) yields the nondimensional relation for the no-mixing boundary layer model,

$$\epsilon = \int_{\xi_0}^{\xi} \left(\frac{d_w}{d\xi}\right)_i \frac{d\xi_i}{\sqrt{y_i - y}} \tag{30a}$$

Substituting equations (26) into equation (24) yields the corresponding relation for the completely mixed boundary layer model,

$$\epsilon = \frac{W^2}{u} \tag{30b}$$

Equations (27) to (30) form a complete set of four equations in four unknowns. The initial conditions for this set of equations are that, at the start of injection of the transpirational fluid into the boundary layer, the boundary layer thickness, mass, and momentum are zero:

$$\epsilon(\xi_0) = 0 \tag{31a}$$

$$W(\xi_0) = 0 \tag{31b}$$

$$u(\xi_0) = 0 \tag{31c}$$

If the flow is not choked flow, the height of the main flow at the start of injection is an independent parameter

$$y(\xi_0) = y_0 \tag{31d}$$

and the problem is an initial-value problem. If the flow is choked, the height of the main flow at the start of injection is dependent on the area of the throat. The area of the throat is unknown since the boundary layer is unknown. The problem is a two-point boundary value problem.

In order to avoid the singularity in equation (30a) and to have finite derivatives at the start of injection, the independent variable is changed from ξ to y. (This assumes that y is a monotonic function of ξ.) Therefore, ξ, ϵ, w, and u are functions of y. Equations (28), (29), and (30a) become

$$W' = Cy\sqrt{y_p - y}\sqrt{1 + (\eta')^2}\,\xi' \tag{32}$$

$$u' = -\frac{\epsilon}{2} \tag{33}$$

$$\epsilon = -\int_{y}^{y_0} W_i' \frac{dy_i}{\sqrt{y_i - y}} \tag{34}$$

The initial condition (31d) comes from equation (27) when ϵ equals zero

$$\eta(\xi_0) = \frac{1}{y_0\sqrt{1 - y_0}} \tag{35}$$

Assume that near the start of injection

$$\epsilon \sim (y_0 - y)^{\alpha}$$

where α is greater than zero since ϵ_0 is equal to zero. From integrating equation (33)

$$u \sim (y_0 - y)^{\alpha+1}$$

When equation (30b) or Abel's solution of equation (37) is used,

$$W \sim (y_0 - y)^{\alpha+(1/2)}$$

From integrating equation (32)

$$\xi - \xi_0 \sim (y_0 - y)^{\alpha+(1/2)}$$

Differentiating equation (27) and substituting yields α equal to 1 as the only finite solution. Therefore, ξ_0', w_0', and u_0' are zero and

$$\epsilon_0' = \frac{2 - 3y_0}{2y_0(1 - y_0)^{3/2}} \tag{36}$$

Equation (36) was derived by differentiating equation (27)

$$\epsilon' = \eta + y\eta'\xi' - \frac{1}{2}(1 - y)^{-3/2} \tag{37}$$

and using the initial values.

Equation (34) is a form of Abel's Integral Equation; and as such, it has an inverse

$$W' = +\frac{1}{\pi}\int_y^{y_0} \frac{\epsilon_i' \, dy_i}{\sqrt{y_i - y}} \tag{38}$$

Numerically, it is convenient if an additional independent variable transformation is made,

$$x_i = 2\sqrt{y_i - y} \tag{39}$$

Then equation (38) becomes

$$W' = +\frac{1}{\pi}\int_0^{2\sqrt{y_0-y}} \left(\frac{d\epsilon}{dy}\right)_i dx_i \tag{40a}$$

The integral in equation (40a) exists if ϵ' is finite. Equation (30b) can be differentiated to give the completely mixed model equivalent of equation (40a),

$$W' = \frac{u\epsilon' + u'\epsilon}{2W} \tag{40b}$$

Equations (28), (29), (37), and (40) form the equation set which is solved numerically. The analytical solution near the start of injection is

$$\epsilon = \epsilon_0'(y - y_0) \tag{41a}$$

$$u = -\frac{\epsilon_0'}{4}(y - y_0)^2 \tag{41b}$$

$$\xi = \xi_0 - \frac{B\epsilon_0'}{C_0 y_0 \sqrt{y_{p,0} - y_0}\sqrt{1 + (\eta_0')^2}}(y_0 - y)^{3/2} \tag{41c}$$

$$W = -B\epsilon_0'(y_0 - y)^{3/2} \tag{41d}$$

where B for the no-mixing case is

$$B = \frac{4}{3\pi} \tag{41e}$$

and B for the complete-mixing case is

$$B = \frac{1}{2} \tag{41f}$$

Equation (40) can be written as

$$W' = F\epsilon' + G \tag{42}$$

where F and G are auxiliary functions. For the completely mixed boundary layer model the auxiliary functions are

$$F = \frac{u}{2W} \tag{43a}$$

and

$$G = -\frac{\epsilon^2}{4W} \tag{43b}$$

For the no-mixing boundary layer model and when the trapezoidal method is used to approximate the integral, the auxiliary functions become

$$F = \frac{\sqrt{-\Delta y}}{\pi} \tag{44a}$$

and

$$G = \frac{1}{\pi} \int_{2\sqrt{-\Delta y}}^{2\sqrt{y_0 - y}} \epsilon_0' \, dx_i + \epsilon' \Big|_{y-\Delta y} \frac{\sqrt{-\Delta y}}{\pi} \tag{44b}$$

Equations (32), (37), and (40) can be solved simultaneously for ξ' and the result is

$$\xi' = \frac{2F\eta - F(1 - y)^{-3/2} + 2G}{2Cy\sqrt{y_p - y}\sqrt{1 + (\eta')^2} - 2Fy\eta'} \tag{45}$$

By using the initial conditions (eqs. (36) and (41)) the differential equations (32), (33), (37), and (45) can be solved numerically by the "Predictor-Corrector Method."

DISCUSSION

The analysis of a water table simulation of a transpirationally cooled nozzle is given in the previous section of this report. The results of this analysis are in the form of four relations. The first is a relation governing the flow through any water table channel, and the next three are relations governing the boundary layer thickness, mass, and momentum. The equations are coupled by the fact that the free-flow channel is equal to

the physical channel minus the boundary layer thickness and also by the fact that the pressure (or height) in the boundary layer is the same as in the main flow. Two boundary layer models were assumed; first, no mixing and, second, complete mixing in the boundary layer.

In order to check the validity of this analysis, a calculation was made for the water table of Perkins and Kinney. A "plan view" of the nozzle walls for this water table is shown in figure 3. The main flow and the flow through sections 1, 2, and 3 were metered. The flow through sections 1 to 3 was dyed and, when photographed, appeared darker than the undyed main flow. Experimental results were recorded photographically for the case of the main flow being equal to 2.27 kilograms per second (5.0 lbm/sec) and the flow through sections 1, 2, and 3 being equal to 0.227, 0.227, and 0 kilograms per second (0.5, 0.5, 0 lbm/sec), respectively.

For this case the calculation was done in the following fashion: First, it was assumed that there was no boundary layer adjacent to the channel wall, ($\epsilon = 0$). The height of the flow y was calculated by using equation (27). With this height, the mass flow rate in the boundary layer W was calculated by using equation (32). These two results were then substituted into equation (34) and a new boundary layer thickness ϵ was calculated. The process was repeated, with the new value of the boundary layer thickness, until there was no change from one iteration to the next. An instability arose in the vicinity of the throat and a smoothing technique was applied so that the position of the throat (critical flow) was stable.

Figure 4 shows the plan view of the water table nozzle. It shows the position of the channel wall and the adjacent boundary layer as a function of axial position, from the start of injection down past the physical throat. The flow is choked, and as such the physical throat and critical flow do not necessarily occur at the same axial position. In general, the boundary layer thickens rapidly near the start of injection and thins somewhat in the high-acceleration region near the throat. The transpiration fluid in general increases the radius of curvature near the throat and decreases the divergence angle downstream of the throat. This suggests that the physical radius of curvature at the throat can be made much smaller and the physical divergence angle can be made larger for a transpirationally cooled nozzle than for a conventional nozzle.

Figures 4(a) to (f) show the results for various iterations. The change is small for the first two iterations and is negligible for the next four iterations. On the sixth iteration, instabilities build up (even though a smoothing routine is used) and cause numerical difficulties in the vicinity of the throat.

These calculations were compared to the experimental results shown in figure 5. In the photograph there is some problem with parallax, and therefore only general trends can be considered. In general, the calculated boundary layer is in close agreement with the photographed boundary layer. The region of largest disagreement is just upstream of the throat and is probably caused by two-dimensional effects.

The preceding calculations were for the no-mixing boundary layer model. Similar calculations were made for the completely mixed boundary layer model, and these results are very close to those shown in figure 5. Figure 6 shows the difference between the two models near the start of injection. The boundary layer thickness, mass, and momentum are plotted as a function of axial distance from the start of injection. In general, both models give similar results. The largest difference occurs in the boundary layer thickness. A smaller difference occurs in the boundary layer momentum; and no difference occurs in the boundary layer mass. These results are, in general, also true farther downstream, as shown in figure 7.

Figure 7 shows the results of the analysis for a simplified geometry. The geometry considered was straight convergent channel walls at a angle of 45^{o} to the centerline. The channel walls, if extended, would have met at the origin of the axial coordinate. The channel wall discharge coefficient was assumed to be 0.01. The stagnation height outside the channel wall was assumed to be equal to the main-stream stagnation height. The problem was an initial-value problem in which the initial nondimensional height was assumed to be 0.95, 0.90, 0.80, and 0.70. The problem was solved from the initial point to the point of choked flow for both models considered in the analysis.

Figure 7(a) shows the nondimensional mainstream height as a function of nondimensional axial distance. The main-stream height is essentially the same for the four different starting conditions. In this case the boundary layer does not influence the main stream very much, or the flow is weakly coupled. The reason for this is that the boundary layer thickness is small compared to the channel width. This is shown in figure 7(b).

Figure 7(b) shows the nondimensional boundary layer thickness as a function of nondimensional axial distance. From the assumed geometry the channel width is equal to twice the absolute value of the axial distance. The largest boundary layer is about 1 percent of the channel width, and thus has a small effect on the free-flow area. The boundary layer thickens rapidly near the start of injection and thins rapidly near the throat. The reason for this is shown in figure 7(c).

Figure 7(c) shows the nondimensional boundary layer mass as a function of nondimensional axial distance. The curves have almost a constant slope and therefore almost constant mass added to the boundary layer per unit axial length. Near the start of injection, the acceleration (the slope of the height-against-distance curve) is low, and therefore the boundary layer must thicken to accommodate the additional mass. Near the throat the acceleration is large, and therefore the boundary layer thins. This acceleration near the throat is shown in figure 7(d).

Figure 7(d) shows the nondimensional boundary layer momentum as a function of nondimensional axial distance. Near the start of injection the change in momentum is small. Near the throat the change in momentum is large.

Figure 8 shows a strongly coupled case. That is, the boundary layer greatly affects the main flow. The case considered was the same as in figure 7, except that the dis-

charge coefficient was increased from 0.01 to 0.1. This resulted in more mass in the boundary layer and therefore a thicker boundary layer (which in turn decreased the free-flow area).

In summary, this report presents two simple models for a water table nozzle, including transpirational flow. The models should be applicable in a region where pressure forces dominate over viscous forces (near the throat). The models are simple enough so that extending them to apply to a gas nozzle, including heat transfer and density differences, should be possible.

CONCLUSIONS

Analysis of a water table simulation of a transpiration-cooled nozzle is given in this report. Two boundary layer models were assumed: first, no mixing and, second, complete mixing in the boundary layer. The analysis was compared to photographic data and resulted in the following conclusions:

1. The two boundary layer models predicted the data within 20 percent over most of the range.

2. Both models predicted similar results; but inherent errors precluded a choice as to which model fit the data best.

3. The largest difference between the data and the analysis were caused by two-dimensional effects being omitted from the analysis and by parallax in the photographic data.

4. The largest differences in the two models occurred in the boundary layer thickness. Less differences occurred in the boundary layer momentum; and only a slight difference occurred in boundary layer mass.

5. Transpiration flows of the order of a few percent of the main flow resulted in only slight perturbation of the main flow. Transpiration flows of the order of tens of percent of the main flow resulted in major changes of the main flow.

In general, the transpiration fluid increased the radius of curvature near the throat and decreased the divergence angle of the free flow downstream of the throat. Thus, the design of a transpirationally cooled nozzle can incorporate a smaller radius of curvature at the throat and a larger divergence angle.

Lewis Research Center,
National Aeronautics and Space Administration,
Cleveland, Ohio, June 26, 1973,
503-04.

APPENDIX - SYMBOLS

A flow cross-sectional area, m^2

a_* reference length, m

B constant defined in eq. (41e) or (41f)

b width of main flow, m^2

C channel wall discharge coefficient a function of axial position

d nondimensional boundary layer thickness

F auxiliary function defined in eq. (43) or (44)

G auxiliary function defined in eq. (43) or (44)

g acceleration of gravity, 9.8 m/sec^2

h height of flow, m

k constant equal to 0, 1, or 2

$\dot{M}$ momentum flow rate, $kg\text{-}m/sec^2$

$\dot{m}$ mass flow rate, kg/sec

S curved distance along channel wall, m

u nondimensional momentum flow rate

v velocity, m/sec

W nondimensional mass flow rate

x auxiliary independent variable

y nondimensional flow height

z axial distance, m

α exponent used in initial conditions

β nondimensional constant

δ boundary layer thickness, m

ϵ nondimensional boundary layer flow area

η nondimensional channel wall width

ξ nondimensional axial distance

ρ density, kg/m^3

φ angle used in solution of cubic equation

Subscripts:

b	boundary layer
i	injection point
p	plenum
s	stagnation condition
t	throat condition, choked flow
w	wall
1, 2, 3	sections 1, 2, 3
0	start of injection

Superscripts:

(')	differentiation with respect to given independent variable

REFERENCES

1. Ragsdale, Robert G.; and Willis, Edward A., Jr.: Gas-Core Rocket Reactors - A New Look. Paper 71-641, AIAA, June 1971.

2. Howell, John R.; Strite, Mary K.; and Renkel, Harold: Heat-Transfer Analysis of Rocket Nozzles Using Very High Temperature Propellants. Paper 64-62, AIAA, Jan. 1964.

3. Kascak, Albert F.: Nozzle and Cavity Wall Cooling Limitations on Specific Impulse of a Gas-Core Nuclear Rocket. NASA TM X-67923, 1971.

4. Loh, W. H. T.: Theory of The Hydraulic Analogy for Steady and Unsteady Gas Dynamics. Modern Developments in Gas Dynamics. W. H. T. Loh, ed., Plenum Press, 1969, pp. 1-61.

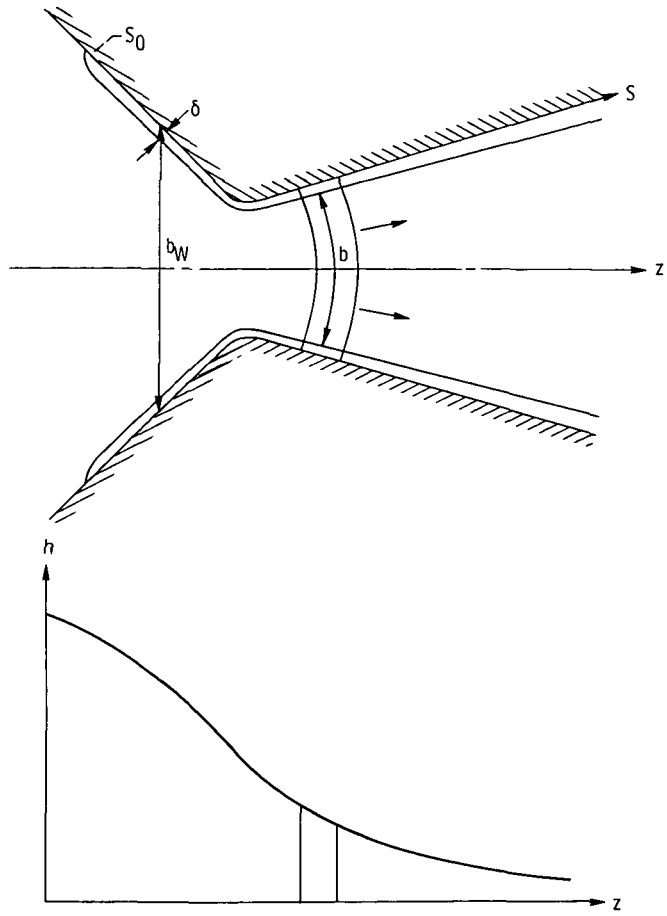

Figure 1. - Plan view of water table nozzle.

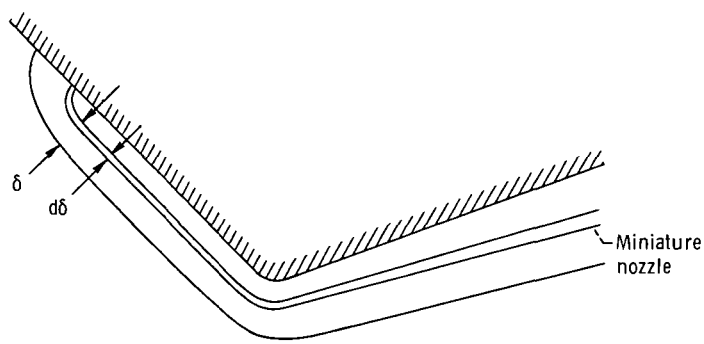

Figure 2. - Closeup of nozzle wall showing no-mixing boundary-layer case.

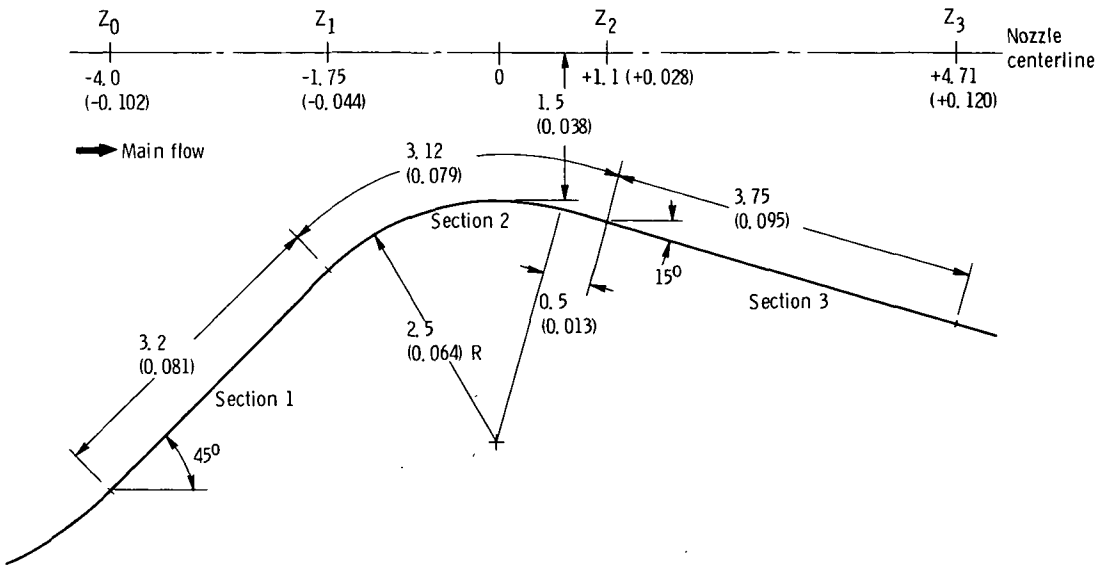

Figure 3. - Plan view of test nozzle used on water table of reference 4. Dimensions are in inches (meters).

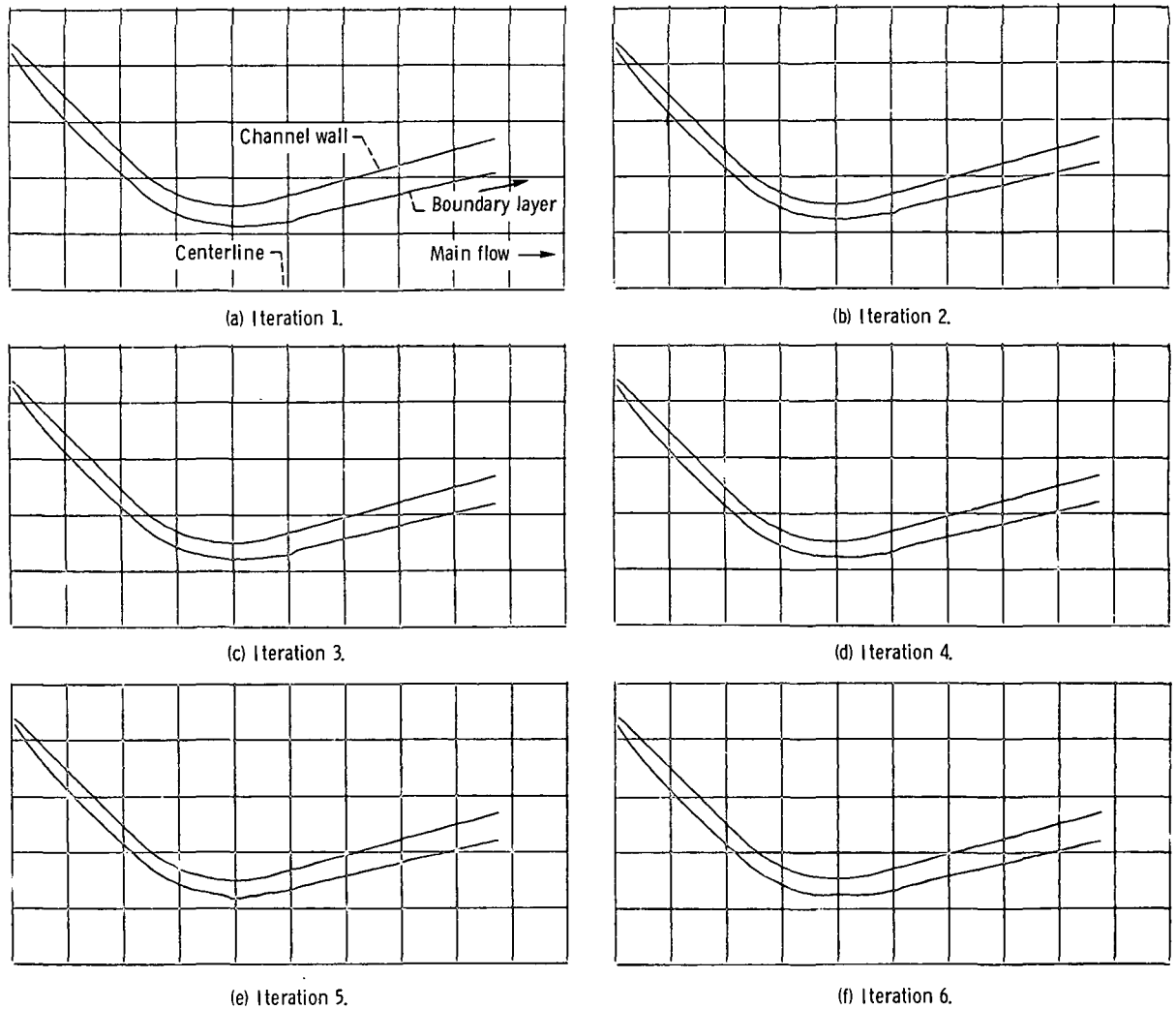

Figure 4. - Plan view of water table nozzle, showing position of channel walls and adjacent boundary layer. Flow rate, kg/sec (lbm/sec): main, 2.27 (5); section 1, 0.227 (0.5); section 2, 0.227 (0.5); section 3, 0 (0).

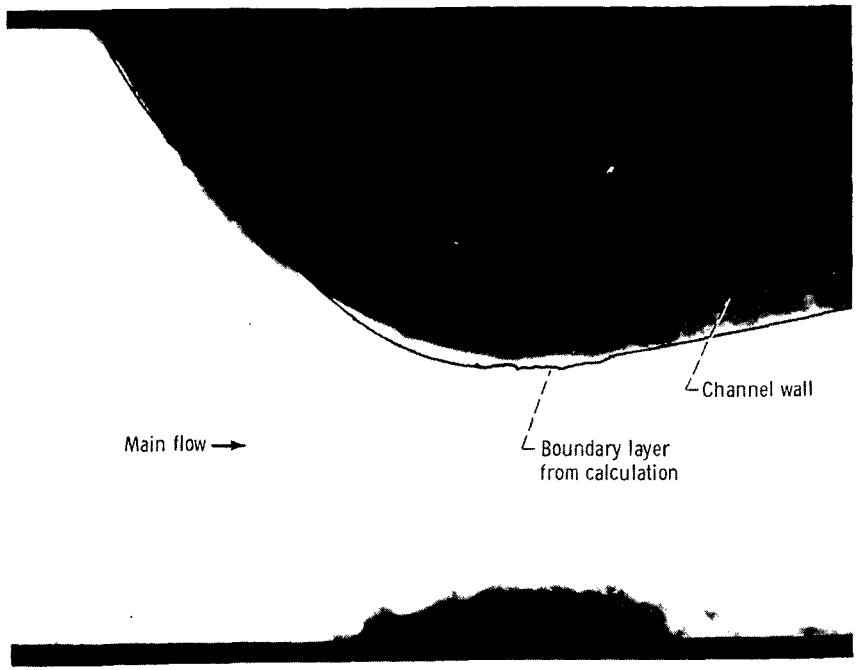

Figure 5. - Water table nozzle, with boundary dyed dark and main flow clear. Flow rate, kg/sec (lbm/sec): main, 2.27 (5); section 1, 0.227 (0.5); section 2, 0.227 (0.5); section 3, 0 (0).

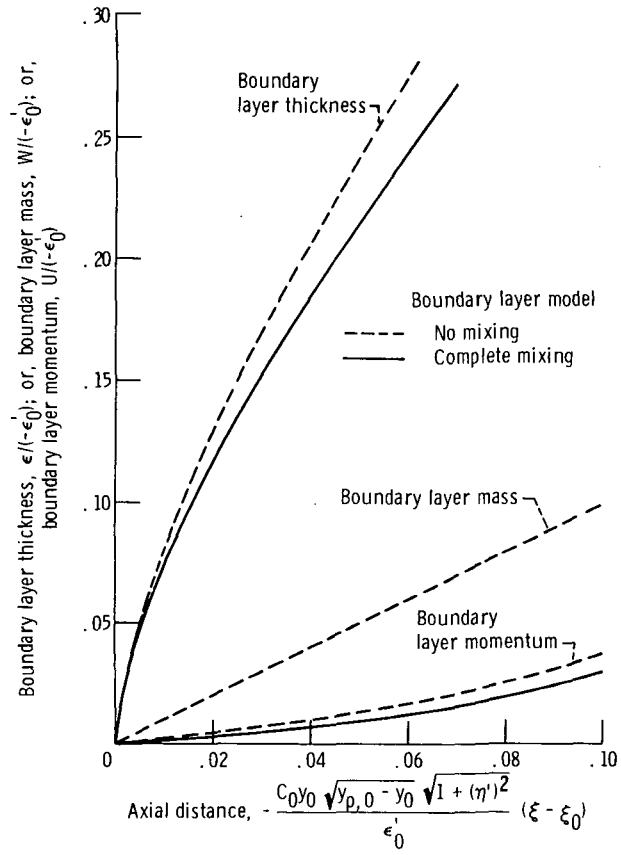

Figure 6. - Boundary layer thickness, mass, and momentum as function of axial distance from start of injection of transpiration flow.

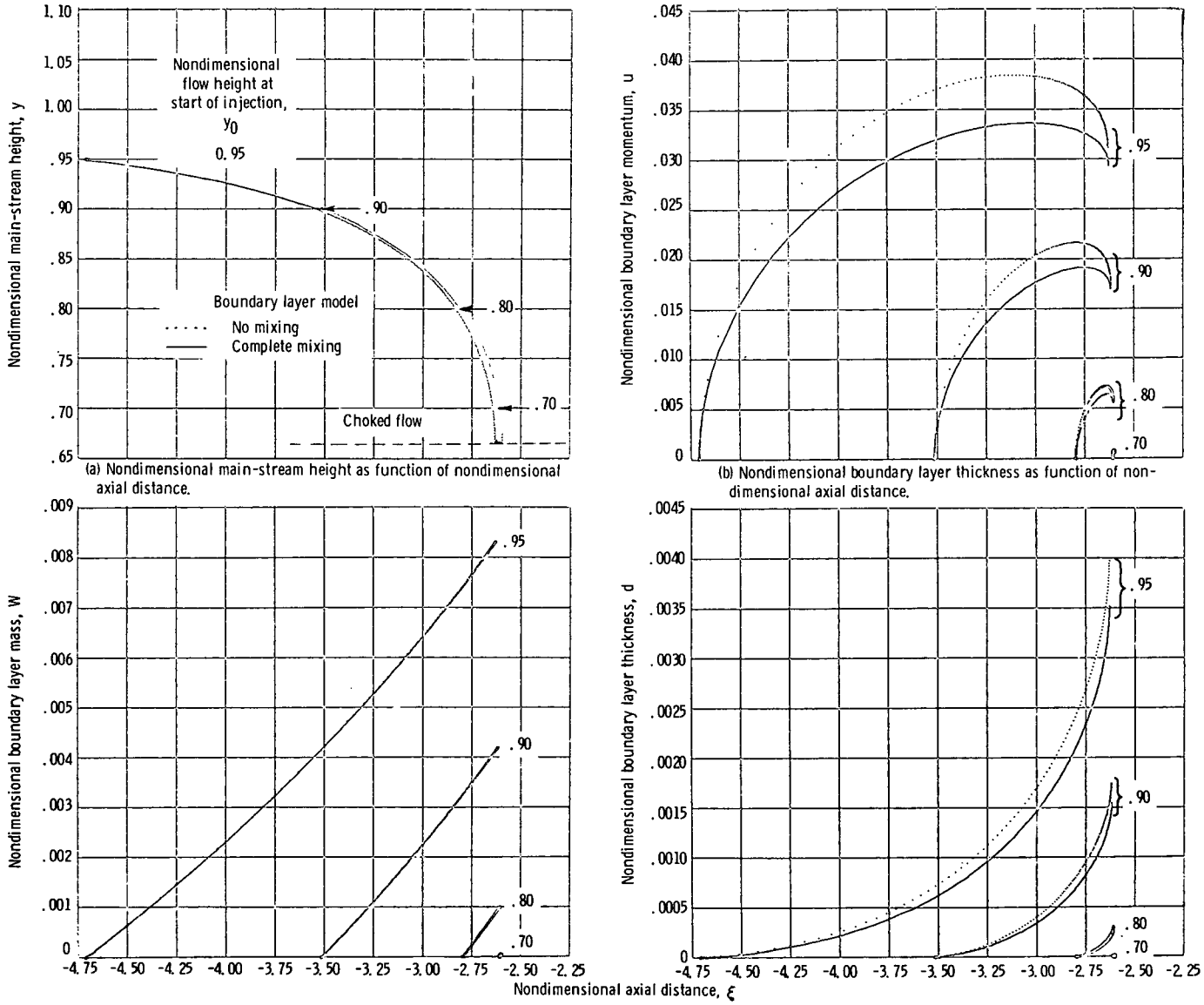

(a) Nondimensional main-stream height as function of nondimensional axial distance.

(b) Nondimensional boundary layer thickness as function of nondimensional axial distance.

(c) Nondimensional boundary layer mass as function of nondimensional axial distance.

(d) Nondimensional boundary layer momentum as function of nondimensional axial distance.

Figure 7. - Solution of transpiration nozzle on water table for weakly coupled case. Channel walls straight and convergent at 45°; discharge coefficient, 0.01; stagnation height outside channel wall equal to main-stream stagnation height; initial main-stream heights, 95, 90, 80, and 70 percent of stagnation.

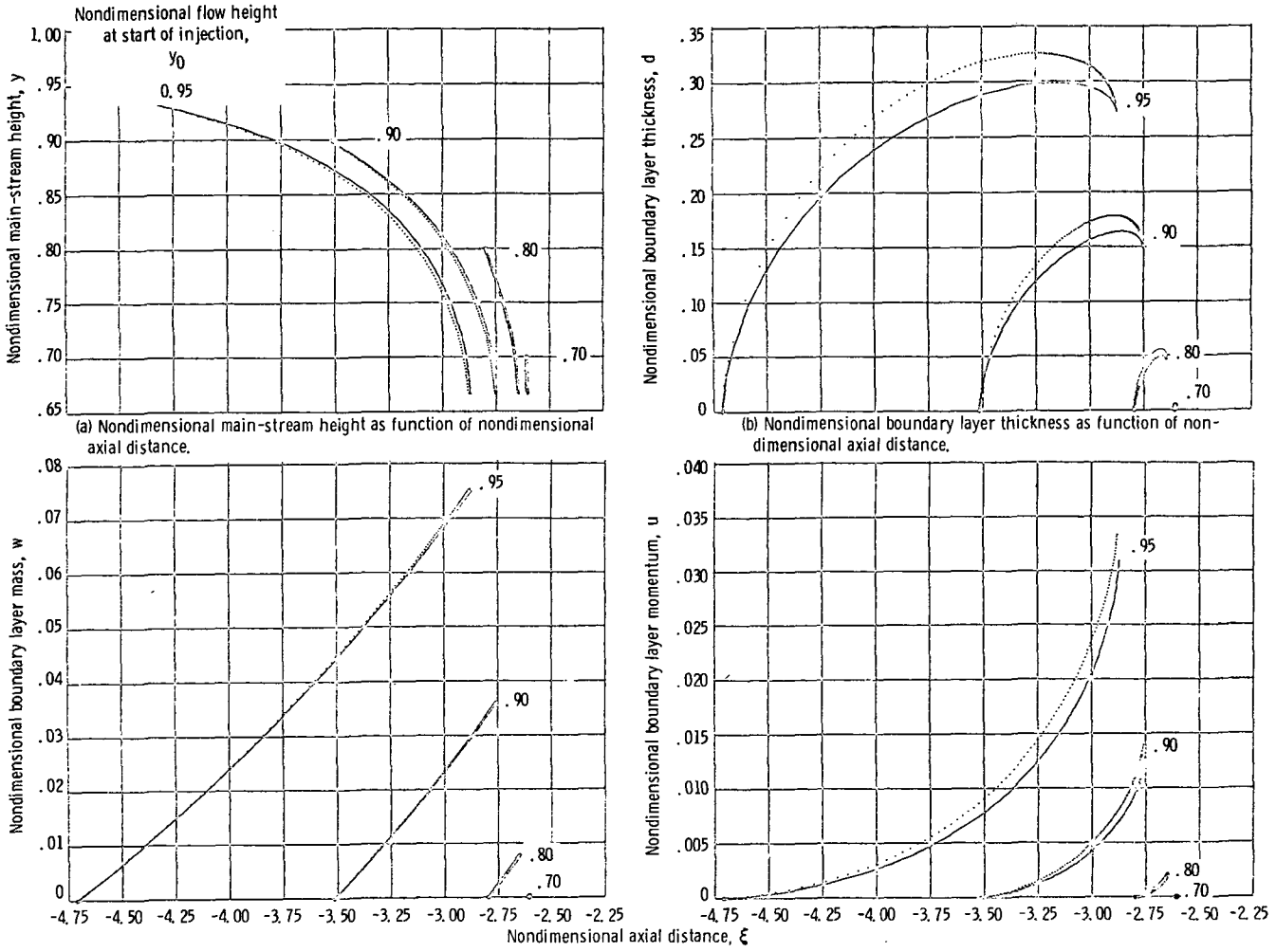

(a) Nondimensional main-stream height as function of nondimensional axial distance.

(b) Nondimensional boundary layer thickness as function of nondimensional axial distance.

(c) Nondimensional boundary layer mass as function of nondimensional axial distance.

(d) Nondimensional boundary layer momentum as function of nondimensional axial distance.

Figure 8. - Solution of transpiration nozzle on water table for strongly coupled case. Channel walls straight and convergent at 45°; discharge coefficient, 0.1; stagnation height outside channel wall equal to main-stream stagnation height; initial main-stream heights, 95, 90, 80, and 70 percent of stagnation.

NATIONAL AERONAUTICS AND SPACE ADMINISTRATION
WASHINGTON, D.C. 20546

OFFICIAL BUSINESS
PENALTY FOR PRIVATE USE $300

SPECIAL FOURTH-CLASS RATE
BOOK

POSTAGE AND FEES PAID
NATIONAL AERONAUTICS AND
SPACE ADMINISTRATION
451

U.S.MAIL

POSTMASTER: If Undeliverable (Section 158 Postal Manual) Do Not Return

"The aeronautical and space activities of the United States shall be conducted so as to contribute . . . to the expansion of human knowledge of phenomena in the atmosphere and space. The Administration shall provide for the widest practicable and appropriate dissemination of information concerning its activities and the results thereof."

—NATIONAL AERONAUTICS AND SPACE ACT OF 1958

NASA SCIENTIFIC AND TECHNICAL PUBLICATIONS

TECHNICAL REPORTS: Scientific and technical information considered important, complete, and a lasting contribution to existing knowledge.

TECHNICAL NOTES: Information less broad in scope but nevertheless of importance as a contribution to existing knowledge.

TECHNICAL MEMORANDUMS: Information receiving limited distribution because of preliminary data, security classification, or other reasons. Also includes conference proceedings with either limited or unlimited distribution.

CONTRACTOR REPORTS: Scientific and technical information generated under a NASA contract or grant and considered an important contribution to existing knowledge.

TECHNICAL TRANSLATIONS: Information published in a foreign language considered to merit NASA distribution in English.

SPECIAL PUBLICATIONS: Information derived from or of value to NASA activities. Publications include final reports of major projects, monographs, data compilations, handbooks, sourcebooks, and special bibliographies.

TECHNOLOGY UTILIZATION PUBLICATIONS: Information on technology used by NASA that may be of particular interest in commercial and other non-aerospace applications. Publications include Tech Briefs, Technology Utilization Reports and Technology Surveys.

Details on the availability of these publications may be obtained from:

SCIENTIFIC AND TECHNICAL INFORMATION OFFICE

NATIONAL AERONAUTICS AND SPACE ADMINISTRATION

Washington, D.C. 20546